UNIVERSITY OF LEEDS

Analysis of Super Knock and Detonation in A Rapid Compression Machine

Jinzhou Li, Junfeng Yang

School of Mechanical Engineering, University of Leeds, Leeds LS2 9JT, United Kingdom

1   Introduction

The engine super knock limits the application of higher compression ratios on modern engines with high thermal efficiency [1]. It is therefore necessary to understand the knock characteristics for the applications in advanced engines with high compression ratios. The previous research [2, 3] reported that the super knock with high knock intensity in engine conditions is highly likely caused by developing detonation as the reaction wave coupling with the shock wave. In order to investigate the mechanism of engine knock and its influencing factors, numerous experimental works have been conducted on the engines [1] and Rapid Compression Machine (RCM) [2-5]. In present study, the Leeds optical RCM with high-speed camera system was implemented to record the pressure traces and corresponding combustion images of two different fuels, i-octane (RON = 100) and coal-based naphtha (RON = 54), to investigate the mechanism of super knock and developing detonation. The coal-based naphtha with low RON is a promising alternative fuel for engines operating under advanced combustion modes, e.g. HCCI, simultaneously improving the thermal efficiency, and reducing the carbon emissions [6]. The detailed technical specifications of coal-based naphtha were reported in [7].

Besides the experimental works, a theoretical approach based on the Zeldovich hot spot theory [8] has been developed by Bradley et al. [9, 10]. This approach uses two dimensionless parameters ξ and ε to characterize the combustion modes including deflagration, subsonic autoignition and detonation. This approach is adopted in present study to quantify the combustion modes of both i-octane and naphtha.

2   Experimental Setup

All experiments discussed in the present work were conducted by Leeds optical RCM. The configuration of Leeds RCM rig shown in Fig. 1 consists of combustion chamber, hydraulic damped chamber, pneumatic driving reservoir, displacement laser system and the mixing chamber. It employs a creviced piston to reduce the effects of aerodynamic mixing during the compression process, and is configured for a wide range of pressures, P_{eoc}, (1-3 MPa) and temperatures, T_{eoc}, (600-1000 K) at the End of Compression (EOC). The fuel, oxygen and dilution gases (Ar, N_2 and CO_2) were homogeneously mixed through the partial pressure method and heated in a 1.8 L stainless steel mixing chamber. The combustion chamber is evacuated to a maximum absolute pressure of 20 mbar and the mixtures inside the mixing chamber is filled into the combustion chamber due to the pressure difference and the volume of inlet mixtures is based on the partial pressure method. Thereafter, the 1.35 MPa cylinder air in the

pneumatic driving reservoir drives the creviced piston moving forward to reach the target P_{eoc} and T_{eoc}. The end of the combustion chamber is fitted with an optically flat, fused silica window (69 mm diameter × 40 mm thick). A dynamic pressure transducer (Kistler 6045A) was flush-mounted on the cylinder wall to record the in-cylinder pressure signal with a sampling rate of 100 kHz.

A monochrome high-speed CMOS camera (Photron Fastcam SA1.1) with a Tokina AT-X PRO lens with 2.8 aperture positioned immediately in front of the quartz window to record the radiations from the evolving reactions with resolution setup of 256 x 256 pixels. The framing rate was 67,500 frame per second (fps) with pixel size of 0.176 mm/pixel. The shutter speed maintained at 14.81 μs. The focal plan is focused on the piston front which located at the EOC position. The calibration work is performed by matching the pixel size and focal plan.
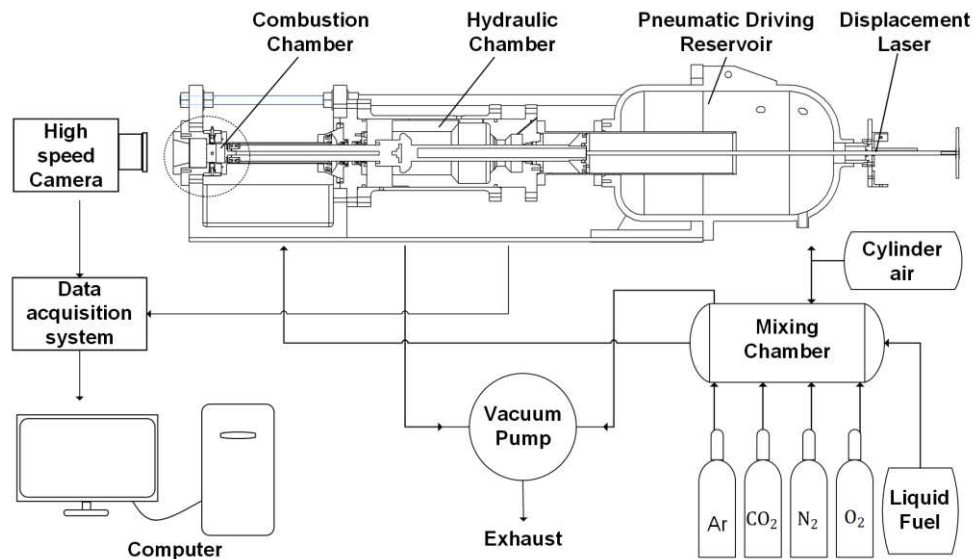

Figure 1: The overall layout of Leeds optical RCM rig and high-speed camera system.

3   Results and Discussions

3.1 Detonation Images and Pressure Records

The pressure trace and the monochrome images showing the super knock and developing detonation for stoichiometric naphtha at T_{eoc} = 770 K with two different values of P_{eoc} at 1 and 2 MPa, are presented in Fig. 2 and 3, respectively. Shown in Fig. 2 (d) and (e), as the reaction wave approached the cylinder wall, it bounced back towards the center of cylinder, generating the super knock (indicated by the peak pressure). The super knock is caused by the reflection of reaction wave, and this finding is consistent with the study of *i*-octane explosion experiment in [2].

At the higher P_{eoc} with 2 MPa in Fig. 3, the autoignition (AI) point initiated at the left-top side of cylinder wall and propagated toward the center of cylinder. At 0.09 ms, as shown in image (g), two bright detonation pulses ahead of reaction wave were observed, and point (g) on the pressure trace indicates that the onset of super knock is caused by the initiation of detonation pulses. Shown in Fig. 4, the AI of *i*-octane explosions initiated at the bottom of cylinder and propagation into the top of cylinder. The onset of detonation pulse is caused by the new AI spot ahead of reaction wave captured by the high-speed camera, see Fig. 4 (f). The new AI spot is induced due to the compression effect of reaction wave on the unburned gas located at the corner of cylinder wall, which leads to strong autoignition. This strong autoignition hot spot eventually developed into detonation pulse shown in Fig.4 (h) accompanied by super knock. Wang et al. [2] has conduct detonation experiments in RCM, and observed the initial autoignition reaction wave does not self-accelerate to the detonation. Instead, the detonation pulse is

triggered by the new "hot spot". which referred to "hot spot induced detonation". This detonation initiation mechanism is consistent with the present work, see Fig. 3 (g) and Fig. 4 (h). This mechanism is applicable to both *i*-octane and coal-based naphtha, suggesting that the hot spot induced detonation mechanism might be general for the transition to detonation in all liquid fuels under engine conditions.
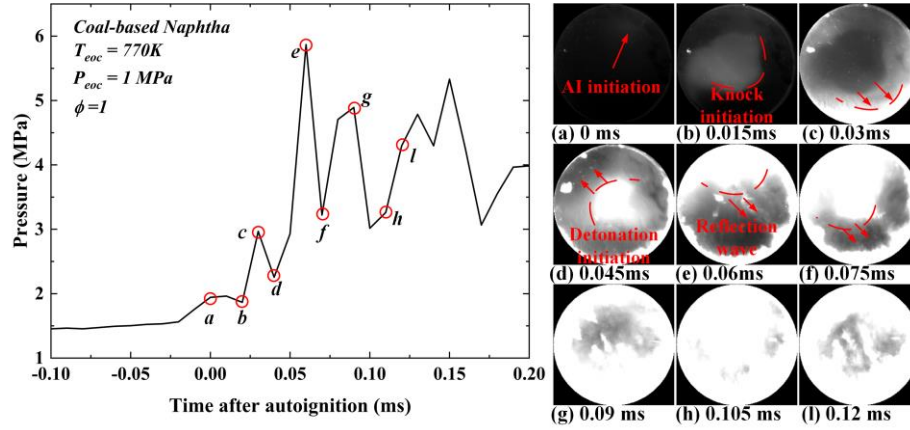

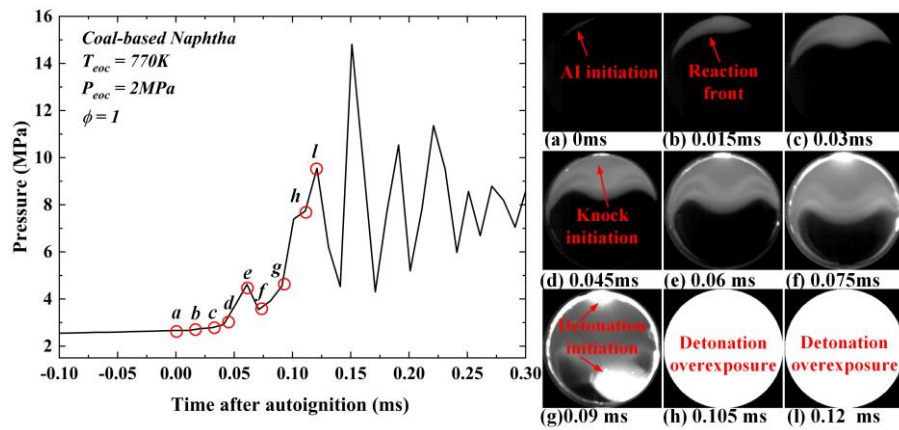Figure 2: Pressure trace and monochrome images of coal-based naphtha at 770 K, 1 MPa and $\phi = 1$.

Figure 3: Pressure trace and monochrome images of coal-based naphtha at 770 K, 2 MPa and $\phi = 1$.
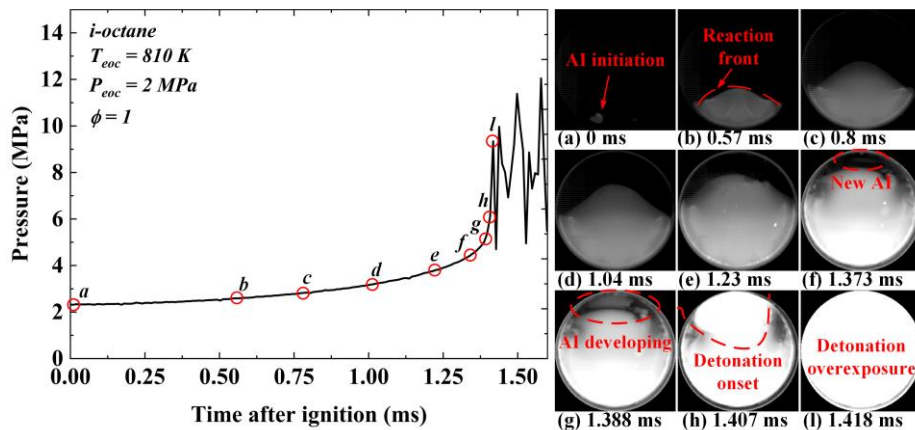

Figure 4: Pressure trace and monochrome images of *i*-octane at 810 K, 2 MPa and $\phi = 1$.

3.2 Detonation Peninsulas

The detonation peninsula is a good tool to access the relative severities of different autoignitions. It is necessary to introduce the two dimensionless parameters ξ and ε here to quantitatively predict the combustion modes to confirm whether the transition to detonation occur. The first parameter ξ is defined as the ratio of local acoustic velocity, a, over the autoignitive velocity, u_a, and its unity value indicates the autoignitive wave coupling with the acoustic wave representing the transition to detonation. The acoustic velocity is calculated from the GasEq code [11]. The autoignitive velocity is based on the Zeldovich hot spot temperature gradient theory [8] expressed as:

$$u_a = \frac{\partial r}{\partial \tau_i} = \left(\frac{\partial r}{\partial T}\right) / \left(\frac{\partial \tau_i}{\partial T}\right). \tag{1}$$

Following the work of [10, 12], the assumption of constant gradient $\frac{\partial T}{\partial r}$ = -2 K/mm is implemented in this study. The i-octane oxidation kinetics embedded in the detailed Lawrence Livermore National Laboratory (LLNL) gasoline chemical kinetics [14] was employed here to calculate the thermo-chemical parameters, e.g. ignition delay time, τ_i, and excitation time, τ_e. For the naphtha, a three-components surrogate model (n-hexane, n-C_6H_{14}: iso-octane, i-C_8H_{18}: iso-heptane, i-C_7H_{16} 62.4: 32.5: 5.1 by mol%) developed by Xie et al. [7] was adopted in this study to match the RON and H/C ratio. The oxidation kinetics of naphtha components are also embedded in LLNL gasoline kinetics [14]. To validate those combustion kinetics, the ignition delay time calculation have been performed using the CHEMKIN's closed homogeneous batch reactor [13].
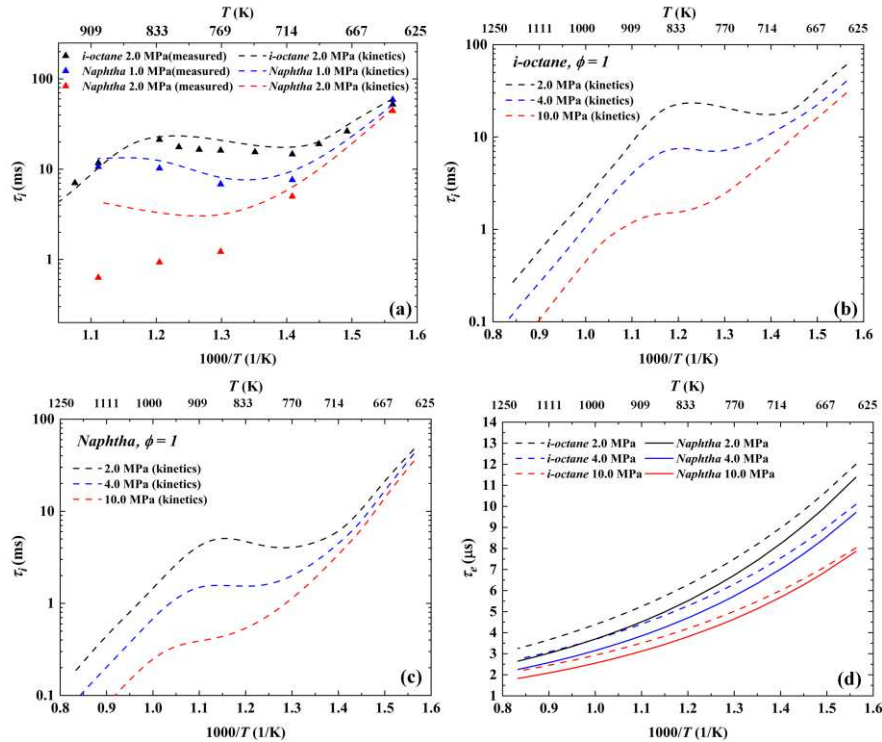

Figure 5: Measured and simulated τ_i for (a) i-octane and naphtha; simulated τ_i for (b) i-octane and (c) naphtha; and simulated τ_e for (d) i-octane and naphtha, plotted against temperature. Symbol represent measured data, while dashed lines correspond to LLNL kinetics data.

The measured ignition delay times (solid triangles) of stoichiometric i-octane and coal-based naphtha at 1-2 MPa are compared with those predicted value (dashed lines) using LLNL gasoline kinetics, see Fig. 5(a). For the i-octane at 2 MPa, the predicted τ_i shows a good fitting with the measurement. Such a good fitting is also observed for naphtha at 1 MPa. As the initial pressure rises to 2 MPa, the kinetics over-predicted τ_i. This over-estimation becomes notable under medium- and high- temperature (770 K – 900 K) ranges. This kinetics have been employed for predicting the τ_i of i-octane (Fig. 5(b)) and

naphtha (Fig. 5(c)) under higher pressure conditions (2-10 MPa) since this pressure range occurs in RCM. The local slope of τ_i plot represents the gradient $\frac{\partial \tau_i}{\partial T}$, which is the key term in Eq.1. A correlation of τ_i as a function of T and P proposed by Kalghatgi et al. [12] is employed here. The second parameter, ε, is relevant to the energy fed rate from a reactive hot spot with radius, r_0, into an autoignitive flow and expressed as:

$$\varepsilon = \frac{r_0}{a\tau_e}. \tag{2}$$

The chemical excitation time, τ_e, is defined as the duration from 5% of the maximum heat release rate to its maximum value [15]. The predicted heat release rate from afore-mentioned ignition delay time calculation is then used to determine the τ_e. The predicted τ_e as a function of temperature and pressure are presented in Fig. 5(d) for both i-octane and naphtha. Following the work of [10, 12], the assumption of $r_0 = 5$ mm is selected in this study to calculate ε.
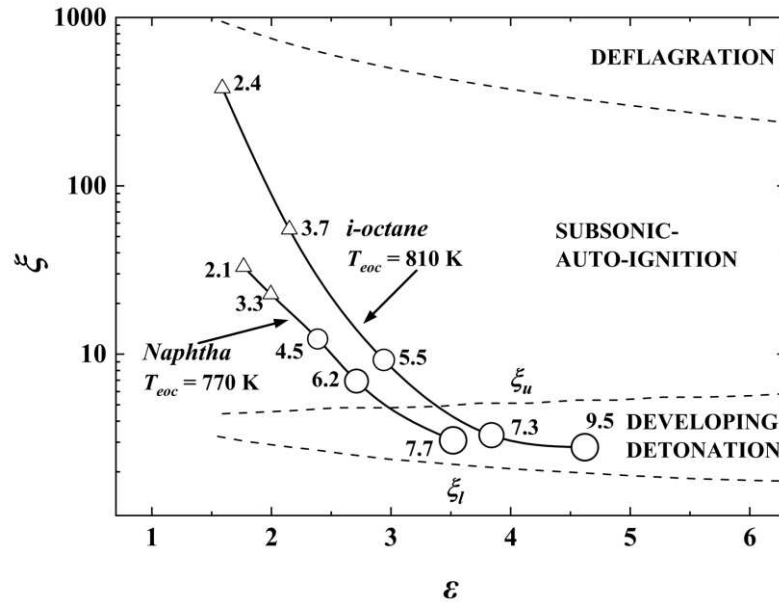

Figure 6: ξ - ε diagram for stoichiometric coal-based naphtha and i-octane.

As shown in Fig 6, the ξ - ε diagram is constructed with the boundaries of three different regimes including Deflagration, Subsonic-Autoignition and Developing Detonation, based on the numerical analysis in [9] and engine experiments in [10]. Fig. 6 shows ξ - ε plots for T_{eoc} values of 770 K for stoichiometric coal-based naphtha, 810 K for stoichiometric i-octane with all P_{eoc} at 2 MPa. For each T_{eoc}, five points of autoignition pressure, P_{ai}, and their corresponding temperature, T_{ai}, based on the isentropic compression law, were selected from the onset of AI to the peak pressure. These points provide the full history of combustion modes as the reaction proceeds. The triangle symbol represents non-oscillation pressure record, and the size of the circular symbol indicates the magnitude of the pressure oscillation amplitude. The number on the right of a symbol is the P_{ai} in MPa during the compression of reaction wave. For the naphtha explosion with $T_{eoc} = 770$ K, it starts in the regime of subsonic autoigintion with P_{ai} at 2.1 MPa and as the reaction proceeding, decrease ξ and increase ε. Finally, as the P_{ai} reaches 7.7 MPa (corresponding image (h) in Fig. 3), this point located inside the developing detonation peninsula indicating the transition to detonation. For the explosions of i-octane with $T_{eoc} = 810$ K, initially the subsonic autoignition predominate the onset of ignition and eventually move inside the detonation peninsula with $T_{eoc} = 810$ K at 7.3 MPa (corresponding image (h) in Fig. 4) indicating the transition to detonation. Overall, this peninsula indicates that the explosions in the current study are initiated by subsonic autoignition, which eventually transitions from autoignition to detonation.

4   Conclusion

In the current study, the propagation of reaction wave, formation of detonation pulse and corresponding pressure trace of stoichiometric coal-based naphtha and *i*-octane were recorded using an optical RCM. The pressure traces and evolution of explosion images in Figs. 2-4 demonstrate that the onsets of super knock are caused by the formation of detonation pulses, which developed by new "hot spot" ahead of reaction wave. Two explosions are located on the ξ-ε diagram, with ignition onsets initiating in the subsonic autoignition regime, characterized by smooth pressure traces. As the reaction proceeds, the system enters the detonation peninsula, exhibiting increasing pressure oscillation amplitude. The super knock pressure traces, detonation pulse images and ξ-ε parameters all support the conclusion that the super knock in RCM is caused by the transition to detonation.

References

[1] Wang Z, Liu H, Reitz RB. (2017). Knocking combustion in spark-ignition engines. Prog. Energy Combust. Sci. 61: 78–112.

[2] Wang Z, Qi Y, He X, Wang J, Shuai S, Law CK. (2015). Analysis of pre-ignition to super-knock: Hotspot-induced deflagration to detonation. Fuel. 144: 222-227.

[3] Pan J, Hu Z, Wei H, Pan M, Liang X, Shu G, Zhou L. (2019). Understanding strong knocking mechanism through high-strength optical rapid compression machines. Combust. Flame. 202: 1-15.

[4] Wang Y, Qi Y, Liu W, Wang Z. (2020). Investigation of methanol ignition phenomena using a rapid compression machine. Combust. Flame. 211: 147-157.

[5] Liu W, Qi Y, Zhang R, Wang Z. (2022). Flame propagation and auto-ignition behavior of iso-octane across the negative temperature coefficient (NTC) region on a rapid compression machine. Combust. Flame. 235: 111688.

[6] Park W. (2021). Naphtha as a fuel for internal combustion engines. Int. J. Automot. Technol.. 22(4): 1119-1133.

[7] Xie Y, Lu A, Li J, Yang J, Zhang C, Morsy M. (2023). Laminar burning characteristics of coal-based naphtha. Combust. Flame. 249: 112625.

[8] Zeldovich YB. (1980). Regime classification of an exothermic reaction with nonuniform initial conditions. Combust. Flame. 39: 211–214.

[9] Gu XJ, Emerson DR, Bradley D. (2003). Modes of reaction front propagation from hot spots. Combust. Flame. 133: 63-74.

[10] Bates L, Bradley D, Paczko G, Peters N. (2016). Engine hot spots: Modes of auto-ignition and reaction propagation. Combust. Flame. 166: 80-85.

[11] Morley C. (2005). GasEq: a chemical equilibrium program for windows; <http://www.gaseq.co.uk>.

[12] Kalghatgi GT, Bradley D, Andrae J, Harrison AJ. (2009). The nature of 'superknock' and its origins in SI engines, In IMechE conference on internal combustion engines: performance fuel economy and emissions 8-9.

[13] CHEMKIN-Pro 19.2. (2017). Reaction Design Inc. San Diego. California.

[14] Mehl M, Pitz WJ, Westbrook CK, Curran HJ. (2011). Kinetic modeling of gasoline surrogate components and mixtures under engine conditions. Proc. Combust. Inst. 33(1): 193-200.

[15] Lutz AE, Kee RJ, Miller JA, Dwyer HA, Oppenheim AK. (1988). Dynamic effects of autoignition centers for hydrogen and C1, 2-hydrocarbon fuels. Proc. Combust. Inst. 22: 1683-1693.